The properties of a gigantic jet reflected in a simultaneous sprite: Observations interpreted by a model

T. Neubert,[1] O. Chanrion,[1] E. Arnone,[2] F. Zanotti,[3] S. Cummer,[4] J. Li,[4] M. Füllekrug,[5] S. Soula,[6] and O. van der Velde[7]

Received 13 June 2011; revised 27 September 2011; accepted 28 September 2011; published 30 December 2011.

[1] Thunderstorm clouds may discharge directly to the ionosphere in spectacular luminous jets – the largest electric discharges of our planet. The properties of these "giants," such as their polarity, conductivity, and currents, have been predicted by models, but are poorly characterized by measurements. A recent observation of a giant, fortuitously illuminated by an unusual sprite discharge in the mesosphere, allows us to study their electric properties and effects on the atmosphere-ionosphere. We show from a first-principles model of the combined giant and sprite event that the observations are consistent with the nature of the giant being a leader in the stratosphere of line charge density $\sim$0.8 mCm^{-1} and of multiple streamers in the mesosphere. It is further shown that the giant modifies the free electron content of the lower ionosphere because of electric field-driven ionization, electron attachment and detachment processes. This is the first time that sprites are used for sounding the properties of the mesosphere. The results presented here will allow evaluation of theories for jet and gigantic jets and of their influence on the atmosphere and ionosphere.

Citation: Neubert, T., O. Chanrion, E. Arnone, F. Zanotti, S. Cummer, J. Li, M. Füllekrug, S. Soula, and O. van der Velde (2011), The properties of a gigantic jet reflected in a simultaneous sprite: Observations interpreted by a model, *J. Geophys. Res.*, *116*, A12329, doi:10.1029/2011JA016928.

1. Introduction

[2] Thunderstorms can discharge upwards into the stratosphere as the so-called "blue jet" [*Wescott et al.*, 1995] or all the way to the ionosphere at $\sim$80 km altitude as the "gigantic jet" [*Pasko et al.*, 2002; *Su et al.*, 2003; *van der Velde et al.*, 2007; *Cummer et al.*, 2009; *Kuo et al.*, 2009; *Chou et al.*, 2010; *Soula et al.*, 2011]. The discharges are named from their appearance in video recordings that show luminous emissions propagating upwards at speeds from 10^5–10^7 ms^{-1} with radii and velocities increasing with altitude. Jets are not directly associated with cloud-to-ground lightning flashes but can be generated spontaneously from charge distributions in the upper layers of thunderclouds [*Wescott et al.*, 1998a]. Theories predict that blue jets most commonly are of positive polarity, transporting net positive charge upwards, and that gigantic jets are of negative polarity, although the reverse polarity may occur for inverted storms [*Krehbiel et al.*, 2008; *Williams*, 2008; *Riousset and Pasko*, 2010]. It has further been proposed that jets are bi-directional leaders, where the body is almost charge neutral with one end of the leader in the cloud and the other propagating upwards [*Mishin and Milikh*, 2008]. More information on jets and gigantic jets are given by *Pasko and George* [2002] and *Pasko* [2003, 2008].

[3] Sprites are discharges in the mesosphere powered by the quasi-electrostatic field following a positive cloud-to-ground (+CG) lightning discharge. The most common sprites, when observed in optical video-rate camera recordings, are the column and carrot sprites, named after their appearance [*Sentman at al.*, 1995; *Wescott et al.*, 1998b; *Neubert*, 2003].

[4] Lightning has two principal modes of discharge, the streamer and the leader. The leader has a high gas temperature that increases detachment of electrons from O_2^-, high ionization and electric conductivity, and propagates at relatively modest velocities of $\sim 10^5$–10^6 ms^{-1}. The streamer has a lower gas temperature, ionization, and electric conductivity, and propagates at velocities of $\sim 10^7$ ms^{-1}. In lightning, many streamers are continuously launched ahead of the leader, feeding the leader and assisting its propagation [*Raizer*, 1997, p. 364]. The breakdown electric field, E_k, is the field magnitude where the ionization rate exceeds the attachment rate. Its magnitude scales with the pressure and is $\sim$3.2 MV/m at ground pressure and $\sim$146 V/m at 70 km [*Raizer*, 1997, p. 135]. A streamer can propagate into regions of the atmosphere where the background field is below E_k because of the enhanced space charge electric field created in the tip of the streamer which adds to the background field.

[5] It is generally accepted that sprites are made up of streamers. Jets, on the other hand, are thought to be leaders

[1]Division for Solar System Physics, National Space Institute, Technical University of Denmark, Copenhagen, Denmark.
[2]Istituto di Scienze dell'Atmosfera e del Clima, CNR, Bologna, Italy.
[3]Italian Meteor and TLE Network, Bologna, Italy.
[4]Department of Electrical and Computer Engineering, Duke University, Durham, North Carolina, USA.
[5]Centre for Space, Atmospheric and Oceanic Science, Department of Electronic and Electrical Engineering, University of Bath, Bath, UK.
[6]Observatoire Mid-Pyrénées, Laboratoire d'Aérologie, Université Paul Sabatier de Toulouse, CNRS, Toulouse, France.
[7]Electrical Engineering Department, Technical University of Catalonia, Terrassa, Spain.

0148-0227/11/2011JA016928

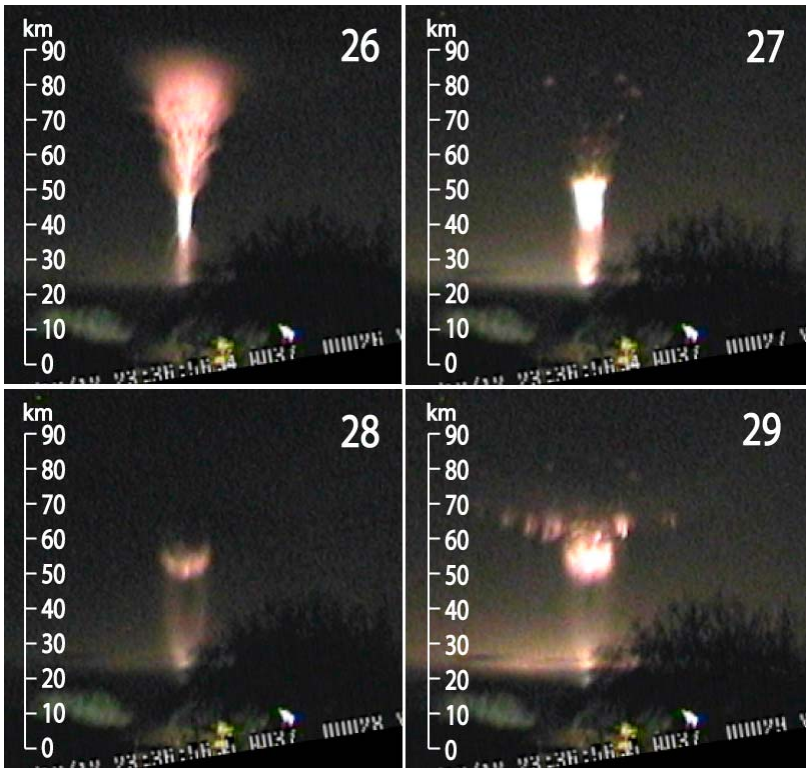

Figure 1. Four consecutive video frames (26–29) of a positive giant observed off the coast of Corsica [*van der Velde et al.*, 2010]. Frame 29 shows the re-brightening of the tip and an unusual series of sprite elements around the tip region.

because their conductivity must be sufficient to enable a significant portion of the cloud electric potential to reach high altitudes in order to sustain the jet discharge [*Pasko and George*, 2002; *Pasko*, 2008; *Raizer et al.*, 2006; 2007; *Milikh and Shneider*, 2008], however, this potential cannot be measured directly.

[6] Here we study a gigantic jet, hereafter referred to as a "giant," observed during a winter thunderstorm over the Mediterranean Sea [*van der Velde et al.*, 2010]. The giant was followed by an unusual sprite generated in close proximity. The shape of the sprite allows us to test the hypothesis of the leader nature of the giant and its perturbation to the electron density and electric conductivity in the mesosphere. In the following we present the observations of the events and a simple first-principles model that is able to capture the main properties of the observations. The model further allows us to understand the relationship between jets, giants and sprites, and their effects on the lower ionosphere.

2. The Observations

[7] The optical and electromagnetic measurements of the giant are described in detail by *van der Velde et al.* [2010]. Here we only emphasize two points: (1) it is the first giant that fortuitously is followed by a sprite, generated by a +CG discharge close to the base of the giant, and (2) the optical observations allow us to study the clear and significant expansion of the giant discharge channel at lower altitudes (<50 km). These features are used to derive some basic properties of the giant.

[8] The optical observations are video camera recordings at 40 ms integration per frame taken from the west coast of Italy. The combined event of the giant and the sprite in four consecutive frames is shown in Figure 1. The giant propagates the complete distance to the ionosphere during frame 26, the first frame of the event, and then relaxes to ∼50–60 km altitude in frame 27, with the "stem" continuing to glow with high luminosity and with expanding diameter. In frame 28 emissions have decreased and remain primarily at the top of the stem, and in the last frame of the event, the tip of the stem re-brightens and an additional crown of sprite emissions appears. The sprite elements are generated by a +CG with 196 kA peak current, within 25 km of the base of the giant [*van der Velde et al.*, 2010]. As we will discuss later, the sprite emissions have an unusual appearance that we propose is caused by the presence of the jet. The diffuse top of the giant is estimated to reach 88 km altitude and the distance of the giant from the observation point 305 km. The errors of these estimates are within −3 to +7% [*van der Velde et al.*, 2010].

[9] The charge transport of the giant is estimated from observations by the Duke University receiver (79.09°W, 35.97°N), recording the field components: BEW, BNS in the ULF band (0.1–500 Hz) [*van der Velde et al.*, 2010]. The band implies a minimal identifiable risetime of 2 ms which appears sufficient to resolve much of the dynamics of giants. The current moment change, $I(t)dl$, where $I(t)$ is the current and dl the altitude over which the current is carried, is shown in Figure 2. The current moment has three distinct pulses, marked P1–P3. The first pulse, P1, corresponds to the full

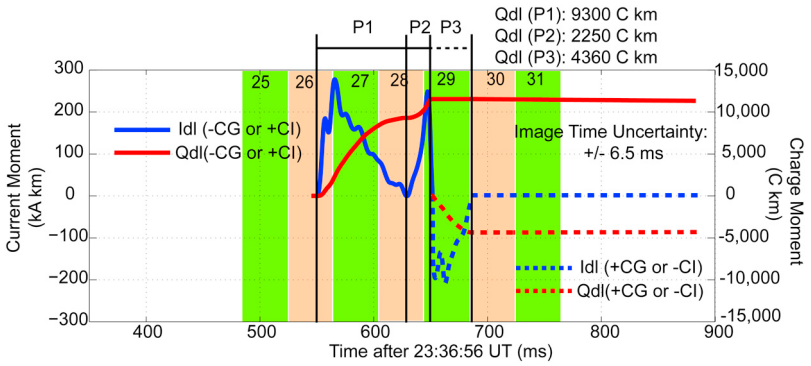

Figure 2. The charge and current moments deduced from the Duke University experiment [*van der Velde et al.*, 2010]. The giant has two current pulses, P1 and P2, carrying net positive charge toward the ionosphere. Pulse P3 corresponds to the positive cloud-to-ground lightning flash generating the sprite of frame 29.

development of the giant in frame 26, P2 occurs during frame 29 and corresponds to the re-brightening of the giant, and P3 is the +CG generating the sprites. Pulses P1 and P2 have positive polarity, and P3 has negative polarity, corresponding to the transport of net positive charge upward in the giant (P1,P2) and downward by the +CG (P3). Alternatively, P1 and P2 could be interpreted as continuing currents from −CG's (negative charge downward); however, two independent lightning detection networks would in this case have missed to detect these rather significant discharges [*van der Velde et al.*, 2010].

[10] According to *van der Velde et al.* [2010], the cloud top altitude for the estimated location of the giant is at 6.5 km. The altitude of the positive charge reservoir is not known, but in the calculations and the model presented in this paper, we assume it is at 6 km altitude. As we shall see, the precise altitude is not important for our conclusions.

[11] The impulsive change in current moment, *Idl*, associated with P3 is from +250 kAkm to −200 kAkm, for a total of 450 kAkm. Comparing this current moment change with the peak current measured by LINET of 198.6 kA, the discharge altitude *dl* must be ∼2.3 km for the two to be consistent. If the positive charge reservoir of the giant and the +CG are in the same region of the cloud, this altitude appears rather low. More likely, the ULF band used to estimate the current moment does not capture the full magnitude of the impulsive peak current of the +CG and therefore the charge region can be higher, but still below the cloud top at 6.5 km altitude. The duration of P3 is almost 40 ms because of the continuing current of the +CG discharge.

[12] The positive charge of the giant is carried to the ionosphere at an estimated altitude of ∼80 km such that $dl \sim 74$ km, and the peak currents of P1 and P2 are $I_o \sim 3.8$ kA and 3.5 kA. The charge moment change, *Qdl*, is also shown in Figure 2. It reaches $\sim 1.2 \times 10^4$ Ckm corresponding to a total net positive charge $Q_o \sim 157$ C carried to the ionosphere during P1 and P2. The total time, t_r, it takes the current moment of P1 to reach its maximum is ∼12 ms. We assume that this risetime is associated with the upward propagation of the jet which reaches its maximum extent at the peak of the current moment of pulse P1. The giant then forms with an average vertical velocity of $v_g \sim 6.2 \times 10^6$ ms^{-1}. The total duration of P1 and P2 is ∼100 ms which corresponds to an average current ∼1.6 kA, a remarkably large value for the global electric circuit which is typically ∼1 kA [e.g., *Rycroft and Odzimek*, 2010]. The parameters derived for the measurements, including the pulse decay time scale, t_d, and the pulse duration, *dt*, are summarized in Table 1.

3. The Model

[13] We adopt a quasi-electrostatic (QE) approach where it is assumed for the magnetic field, $\boldsymbol{B}$, that $\nabla \times \boldsymbol{B} \sim 0$. The source electric field generating a sprite is formed by a +CG that discharges a positive charge distribution of a cloud to the ground. The field of the giant is assumed from a line charge that represents the giant "stem." The source fields are given on analytic form assuming that they are the vacuum electrostatic fields of the instantaneous source charge distribution. The response of the atmosphere/ionosphere to the imposed source electric fields is nonlinear. A numerical algorithm is then adopted, where the response is calculated on a 3D Cartesian grid. The QE formulation is discussed by *Pasko et al.* [1997]. It is appropriate for the system we wish to study here where time scales are longer than the times of impulse propagation to the mesosphere (<1 ms) [*Pasko et al.*, 1999].

3.1. The Basic Equations

[14] The model is based on the Maxwell-Ampere equations:

$$\varepsilon_o \partial \boldsymbol{E}/\partial t + \boldsymbol{J} = \varepsilon_o \partial \boldsymbol{E}^*/\partial t \quad (1)$$

$$\boldsymbol{J} = \sum_\alpha \boldsymbol{J}_\alpha \quad (2)$$

$$\boldsymbol{J}_\alpha = \sigma_\alpha \boldsymbol{E} \quad (3)$$

$$\sigma_\alpha = e n_\alpha \mu_\alpha \quad (4)$$

Table 1. Parameters Derived From ELF Measurements Assuming the Positive Charge Reservoir Is at 6 km Altitude[a]

Pulse	*dl* (km)	I_o (kA)	Q_o (C)	t_r (ms)	v_g (ms^{-1})	t_d (ms)	*dt* (ms)
1 (giant-1)	74	3.8	122	12	6.2E6	68	80
2 (giant-2)	74	3.5	35	18	4.1E6	*	*
3 (+CG/sprite)	6	3.3	700	4	−1.5E6	30	34

[a]Asterisk, interrupted.

where $\boldsymbol{E}^*$ is the source field that builds up from the displacement of charge in the source(s), $\boldsymbol{E}$ the electric field of the atmosphere (the sum of the imposed source field and the field induced by electric currents in the atmosphere/ionosphere) and $\boldsymbol{J}_\alpha$ the electric current density of electrons, one species of positive ions, and one of negative ions. The current densities relate to the electric field through their conductivities, σ_α, which are expressed in terms of the unit space charge, e (positive), the density of the current carrying species, n_α, and their mobility, μ_α. The densities and mobilities, and thereby also the conductivity, depend on the electric field magnitude, making the system nonlinear. The effect of the Earth's magnetic field is ignored, simplifying the conductivity to a scalar.

[15] The densities of the charged species depend on the electric field which drives electron attachment to neutrals, detachment of electrons from negative ions, and ionization. They are given by the continuity equations:

$$-e\partial n_e/\partial t + \nabla\cdot\boldsymbol{J_e} = -e(\gamma_i - \gamma_a)n_e - e\gamma_d n_i \tag{5}$$

$$e\partial n_{i+}/\partial t + \nabla\cdot\boldsymbol{J_{i+}} = e\gamma_i n_e \tag{6}$$

$$-e\partial n_{i-}/\partial t + \nabla\cdot\boldsymbol{J_{i-}} = -e\gamma_a n_e + e\gamma_d n_i \tag{7}$$

where γ_i is the ionization rate, γ_a is the attachment rate, and $\gamma_d n_{N2}$ the detachment rate. They are discussed further in section 3.3.

3.2. The Electric Source Fields

[16] The electric field and charge distributions in thunderstorm clouds can be quite complex. Since we are interested in the electric fields in the mesosphere far from the clouds, we follow a simple approach where the source charge of a region, Q, is approximated by a point source placed at a given altitude within the clouds. We assume, furthermore, that the ionosphere and the ground are perfect electrical conductors. The field at a location $\boldsymbol{a}(x, y, z)$ is then a superposition of the main field of the charge and the field of the infinite number of mirror images of the charge in the conducting ground and the ionosphere. We can neglect the small contributions from far away mirror images and only consider the nearest images in the ground and the ionosphere:

$$\boldsymbol{E}_Q(\boldsymbol{a}) = Q/4\pi\varepsilon_o\left[\boldsymbol{a}_c/|\boldsymbol{a}_c|^3 + \boldsymbol{a}_{cg}/|\boldsymbol{a}_{cg}|^3 + \boldsymbol{a}_{ci}/|\boldsymbol{a}_{ci}|^3\right] \tag{8}$$

where $\boldsymbol{a}_c$, $\boldsymbol{a}_{cg}$, $\boldsymbol{a}_{ci}$ are the vectors to point a from the cloud charge center (positive or negative) and their mirror images in the ground and the ionosphere.

[17] In the model we assume that the mirror altitude of the ionosphere is at 100 km and that the thunderstorm cloud has one negative charge center, Q^-, at 3 km altitude (0, 0, 3 km) and one time-varying positive center, $Q^+(t)$, at (0, 0, z_c), with z_c = 6 km. Initially they have equal but opposite charge, $Q^+(0) = -Q^- = Q$. The total field in point a is then given by a sum of the fields of the two charge centers and their mirror images:

$$\boldsymbol{E}^*(\boldsymbol{a}, t) = \boldsymbol{E}_{Q+}(\boldsymbol{a}, t) + \boldsymbol{E}_{Q-}(\boldsymbol{a}) \tag{9}$$

At distances far from the cloud, the field is small at t = 0 because the positive and negative charges are in balance.

[18] The sprite-producing field, $\boldsymbol{E}_s(\boldsymbol{a}, t)$, is now generated by the discharge of a +CG from the upper charge center to ground which removes charge with a time scale τ_c:

$$Q^+(t) = Q_c\,\exp(-t/\tau_c) \tag{10}$$

The total field from the +CG discharge is then found by combining equations (8)–(10).

[19] With the above configuration we have assumed a polarity of the thunderstorm clouds that is the most prevalent one, with the positive charge layer above the negative one. This is opposite to the inverted configuration proposed for positive giants by *Krehbiel et al.* [2008]. However, as the model here does not attempt to capture the discharge processes in the clouds leading to the giant, the polarity of the storm cloud and the altitude of the charge centers are not important. The deciding parameter for our study is the charge moment change, $Q_c z_c$, which is estimated from the ULF measurements. Finally, the real thunderstorm cloud is probably not charge neutral, but has an overall positive surplus charge that is released through the positive giant and the +CG. Although our formalism is highly simplified, it nevertheless captures important aspects of the fields in the atmosphere above the discharge and has been adopted in the past by many authors [e.g., *Pasko et al.*, 1997].

[20] The field of the giant is estimated from the electrostatic field of the charge distribution in the giant stem. We approximate the volume charge distribution with a line charge density, q_g^o, along the vertical axis of the stem, extending between the cloud charge center (0, 0, z_c) and the upper tip of the line charge $z_g(t)$. The line charge density is the volume charge density integrated over a horizontal cross section of the stem and is given in units of C/m. We assume that q_g^o is constant in altitude and that the tip moves upwards with a constant velocity, v_g, until it reaches a maximum altitude z_{gm}. The coordinate system and the geometry are shown in Figure 3. Note that q_g^o is the net line charge density, i.e., $q_g^o = q_g^+ + q_g^-$. If the giant is a leader, then $q_g^o \ll q_g^+(z)$, $|q_g^-(z)|$.

[21] The vertically oriented line charge density is unaffected by the horizontal radial expansion of the stem seen during frames 26–29 of Figure 1, but is not necessarily constant with altitude and time. The assumptions have, however, no effect on the general principles we want to demonstrate with the model.

[22] If the horizontal distance from the line charge is r, then the field at point a is the sum of the horizontal radial component (E_{rg}) and the vertical component (E_{zg}) as given by *Carlsen* [1967]:

$$\boldsymbol{E}_g(\boldsymbol{a}, t) = q_g^o/4\pi\varepsilon_o r\left[\left(\sin\beta_g(\boldsymbol{a}, t) - \sin\beta_c(\boldsymbol{a})\right)\hat{r} + \left(\cos\beta_g(\boldsymbol{a}, t) - \cos\beta_c(\boldsymbol{a})\right)\hat{z}\right] \tag{11}$$

where β_c is the angle between horizontal and the direction to the lower end of the line charge (0, 0, z_c) and β_g the angle between horizontal and the top of the line charge (0, 0, z_g). The angles are positive toward higher altitudes. At altitudes halfway from z_c to z_g, $\beta_g = -\beta_c$, such that $E_{zg} = 0$, and E_{rg} is at its maximum value at this radial distance. At altitudes above z_g, both β_c and β_g are negative, with $|\beta_g| < |\beta_c|$ such that E_{zg} becomes positive, i.e., directed upwards. In the

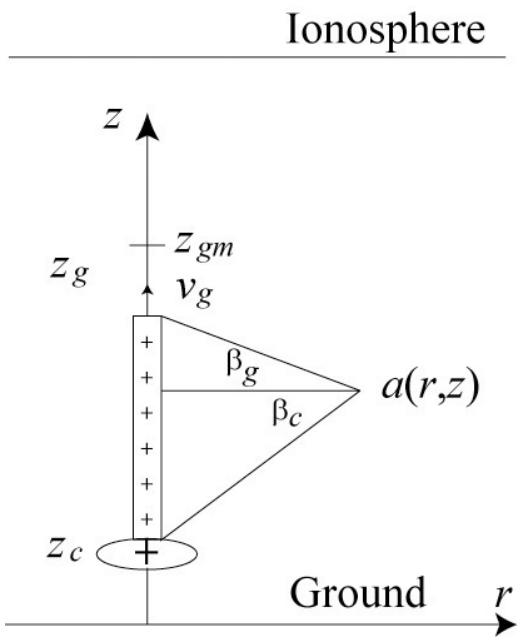

Figure 3. The geometry defining the electric field of the giant (see text).

model, the fields from the negative charge layer and from the mirror charges are included.

3.3. The Conductivity

[23] The electric conductivity of the plasma, $\sigma = \sigma(x, y, z, t)$, is given by the space charge densities, n_α, and mobilities, μ_α. The conductivity defines the decay time of an imposed electric field, the relaxation time, $\tau_\sigma = \varepsilon_o/\sigma(z)$, which decreases with altitude. From this it follows that more impulsive sources are needed for field perturbations at higher altitudes.

[24] The neutral atmosphere is assumed to consist of N_2, O_2 and O, with densities taken from the MSIS-E-90 model (available at http://ccmc.gsfc.nasa.gov/modelweb/models/msis_vitmo.php) for the time and location of the event. The charged component of the background atmosphere is assumed to consist of electrons and positive ions. For the electron density we follow *Cho and Rycroft* [1998]:

$$n_e(z) = n_e^o \exp(z/z_o); z_o = 4.3 \text{ km}, n_e^o = 0.08 \text{ m}^{-3} \quad (12)$$

A positive ion density (singly charged) is added at low altitudes such that the unperturbed electric conductivity is the same as *Pasko et al.* [1997], profile "a."

[25] The perturbation to the background density of the charge-carrying species depends on the electric field which drives ionization of the neutral gas, attachment of electrons to neutral atoms and molecules, and detachment of electrons from negative ions. The threshold field for electric discharge, E_k, is the field strength where the electron production equals the electron loss. It is approximately proportional to the ambient atmospheric neutral density, n_n, such that the so-called reduced electric field, E_k/n_n, is approximately constant.

[26] The primary sink of free electrons in the atmosphere above ~50 km is dissociative attachment to molecular oxygen, given by the reaction

$$O_2 + e^- + 3.7 \text{ eV} \rightarrow O + O^- \quad (13)$$

which depends on the electric field magnitude [*Marshall et al.*, 2010; *Lay et al.*, 2010]. Here we follow *Luque and Ebert* [2010] for the reaction rate, γ_a:

$$\gamma_a = \mu_e^o E \alpha_a \exp(-\beta_a E_k/E) \quad (14)$$

$$\alpha_a = 2 \times 10^3 \text{m}^{-1}; \beta_a = 0.937$$

where μ_e^o is the mobility at sea level. Further discussions on the attachment rate are found in the works of *Pasko et al.* [1998a, 1998b] and *Marshall et al.* [2010].

[27] We consider two sources of electrons: one is impact ionization of atmospheric molecules and the other is detachment from negative ions. The ionization rate, also from *Luque and Ebert* [2010], is taken to be

$$\gamma_i = \mu_e^o E \alpha_i \exp(-\beta_i E_k/E) \quad (15)$$

$$\alpha_i = 4.332 \times 10^5 \text{m}^{-1}; \beta_i = 6.25$$

The attachment and ionization rates have a constant ratio with altitude (density) for a given electric field. For $E = E_k$ they are within a few per cent of each other.

[28] For detachment we follow *Gordillo-Vázquez and Luque* [2010] where the dominant process is found to be

$$O^- + N_2 => N_2O + e \quad (16)$$

The detachment rate is given by *Rayment and Moruzzi* [1978] and characterizes detachment by non-exited N_2 molecules. It has been experimentally determined for fields up to the breakdown field where it approaches 10^{-18} m^3s^{-1} for high fields. A fit to the data of their Figure 4 is:

$$E \le E_k : \gamma_d = n_{N2} \alpha_d \sqrt{E/E_k} \exp(-\beta_d E_k/E) \quad (17)$$

$$\alpha_d = 1.038 \times 10^{-18} \text{ m}^3\text{s}^{-1}; \beta_d = -7.8375 \times 10^{-2}$$

$$E > E_k : \gamma_d = n_{N2} \times 10^{-18} \text{ m}^3\text{s}^{-1} \quad (18)$$

where n_{N2} is the number density of N_2. We assume that the detachment rate is constant for higher fields. The possible error introduced by this assumption is limited because the model is not following the discharge process that occurs at these high fields and therefore the run is stopped shortly after such fields are observed.

[29] The above processes are those that are believed to be dominant at altitudes above ~40 km. Recombination and three body attachment, which are important at lower altitudes, have been neglected.

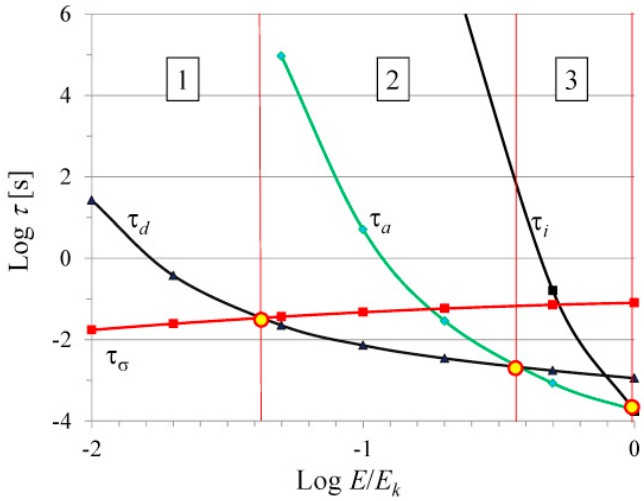

Figure 4. Time scales as functions of the normalized electric field at 70 km altitude. In region 1 the background plasma conductivity has the dominant influence (smallest time scale). In region 2, the detachment process dominates, in region 3, attachment, and above the threshold electric field, ionization.

[30] To calculate the conductivity we also need the mobilities. For the positive and negative ion mobilities we use values from *Chauzy and Soula* [1999]:

$$\mu_{\pm}(z) = (n_n^o/n_n(z))\mu_{\pm}^o \tag{19}$$

$$\mu_+^o = 1.5 \times 10^{-4}\ \mathrm{m^2V^{-1}s^{-1}}$$

$$\mu_-^o = -2.0 \times 10^{-4}\ \mathrm{m^2V^{-1}s^{-1}}$$

where $n_n(z)$ is the total neutral atmospheric number density and n_n^o the density at sea level ($2.57 \times 10^{25}\mathrm{m}^{-3}$). For the electron mobility we follow *Pasko et al.* [1997] (equation (5) and Figure 7) that use the mobility of *Davies* [1983]:

$$\mu_e(z) = (n_n^o/n_n(z))\mu_e^o(z) \tag{20}$$

$$E/E_k \geq 5.063 \times 10^{-4}:$$
$$\mu_e^o(z) = \exp\left(\beta_o + \beta_1\eta + \beta_2\eta^2\right)\ \mathrm{m^2V^{-1}s^{-1}}; \tag{21}$$

$$\eta = \ln(E/E_k);\ \beta_o = -3.229;\ \beta_1 = -0.1299;\ \beta_2 = 0.0441$$

$$E/E_k < 5.063 \times 10^{-4}: \mu_e{}^o(z) = 1.36\ \mathrm{m^2V^{-1}s^{-1}} \tag{22}$$

The formulation is recast from that presented by *Pasko et al.* [1997] but is otherwise the same.

[31] The time constants of the processes are shown in Figure 4 as functions of the normalized electric field E/E_k for 70 km. The time constant associated with the conductivity of the atmosphere, $\tau_\sigma = \varepsilon_o/\sigma$, has the weakest dependence on the field. It continues to decrease with decreasing field until $E/E_k = 5.063 \times 10^{-4}$, below which it is held constant at $1.36\ \mathrm{m^2V^{-1}s^{-1}}$ (equation (22)). In the low field limit and at this altitude $\tau_\sigma = 2.37$ ms.

[32] The timescales associated with electric field driven attachment, ionization, and detachment are $\tau_a = 1/\gamma_a$, $\tau_i = 1/\gamma_i$, $\tau_d = 1/\gamma_d$. When an imposed field increases in the region, the background plasma will first tend to reduce the field. If the field continues to grow, electrons on O^- will detach which tends to increase the conductivity and further reduce the field. (In our model, there is initially no O^-; these ions are created by the attachment process). If the field continues to increase, attachment will dominate, thereby decreasing the free electron content until the field passes the threshold field, where ionization will dominate and additional electrons are brought into play. When the field decreases again, electrons first attach, then detach again until the field vanishes. Which process that will dominate, and in which condition the region is left after being exposed to an electric field pulse, depend on the field amplitude and its temporal variation. We return to a discussion of the detachment process in section 5.

3.4. The Numerical Algorithm

[33] The equations are solved on a 3D Cartesian grid of $100 \times 100 \times 100$ points with 1- km distance between the grid points. The x- and y- axis are horizontal and the z-axis is vertical (positive upwards). At the beginning of each time step, i, we know the electric field, E^i, and the densities, n_α^i. From the electric field we calculate the mobilities, μ_α^i (equations (19)–(22)), and the ionization, attachment and detachment rates, γ_α^i (equations (14), (15), (17), and (18)). Then we find the conductivities, σ_α^i (equation (4)), and the currents, J^i (equation (3)). The new electric field, E^{i+1}, is now updated from the currents and the source electric field, E^{*i+1}- E^{*i} (equation (1)), and the densities, n_α^i, are updated from the ionization rates and the currents (equations (5)–(7)). A similar method is described in detail by *Kulikovsky* [1994]. In our algorithm we adopt an exponential scheme for the update of the field and the densities.

[34] The model does not capture the formation and propagation of the cloud-to ground discharge, the giant propagation, and the discharges of the sprite streamers. Although the physical processes needed to describe these discharges are represented in the model, the grid-resolution is too coarse and we are required to halt the simulation when gradients in the densities cause numerical problems. A model of the complete system would require adaptive grids as in the work of *Luque and Ebert* [2010].

[35] The formulation of the source electric fields are not valid in the region very close to the cloud charge or the leader stem where the field goes to infinity for r going to zero. We circumvent this problem by suppressing the reactions of the atmosphere inside a cylinder around the stem-axis of radius 10 km, topped with a half-sphere around the tip of the stem. It means that inside this region, there are no neutralizing currents flowing to the giant stem, which then maintains it's potential. The equivalent physical situation would be a giant stem that continues to conduct a current from the cloud charge reservoir which balances the current from the atmosphere, thereby maintaining its net space charge. From Figure 1 we see that the tip formed during P1 continues to glow with reduced luminosity for several frames, suggesting

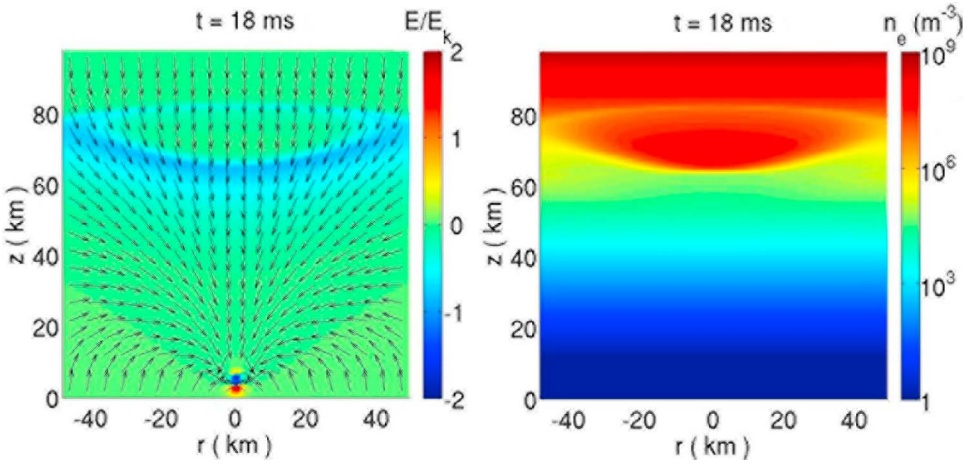

Figure 5. A cloud-to-ground discharge at $t = \tau_c = 18$ ms, with $Q_c = 700$ C and $z_c = 6$ km. (left) The spatial distribution of the normalized electric field, E/E_k. The color shows the magnitude and the arrows the field direction. The color code reflects the sign of the vertical component where an upwards component is positive and a downward component negative. (right) The electron density.

a partial, but decreasing, potential. As we will discuss more later, our treatment of the near-field of the tip is not important for the regions at further distance where the sprite elements are observed. With our approximation we are then able to estimate the line charge needed to modify the appearance of the sprite as observed at some distance from the tip of the giant stem and to understand the response of the mesosphere to the source electric fields.

[36] The model is not a complete ion chemical model, but does account for the dominant exchange between free electrons and O^- ions given by reactions (13) and (16). The minimum time step is chosen for the above processes to be represented down to 40 km altitude.

4. The Results

[37] This section presents the results obtained with those model parameters that give the closest approximation to the optical and electromagnetic data, and having physically plausible values. We first present the results for the +CG that triggers the sprite, then the results for field associated with the giant, and finally we combine the two and compare with the observations.

4.1. Sprite Only

[38] The cloud is assumed to have a positive charge reservoir that feeds the +CG. The electric field of the +CG is modeled using $\tau_c = 18$ ms, $Q_c = +700$ C and $z_c = 6$ km. With these parameters we match the charge moment change estimated from the ULF measurements summarized in Table 1. The time constant of the exponential decay of equation (10) is chosen to fit the decay of the continuing current of P3 (Figure 2), which brings the current moment to a negligible level after 40 ms, as observed. We do not expect the detailed current waveform to be significant for our first-principles model where the QE field, and thus the charge moment change, is the important driver. A matching and undisturbed negative charge reservoir is assumed at $z = 3$ km.

[39] The normalized electric field, $E(r, z)/E_k(z)$, is shown in Figure 5 (left), at $t = \tau_c$. The normalized field reaches a maximum in the mesosphere because the neutral density, and therefore $E_k(z)$, decreases more rapidly (exponentially) with altitude than the source electric field $E_s(r, z)$. The plasma "shorts out" the field at higher altitudes in the ionosphere where $\tau_\sigma \ll \tau_c$. We applied the sign of the vertical E_z –component to the field magnitude shown in Figure 5 in order to illustrate the regions where the field has a component pointing downward (negative) and upwards (positive). The field is above the threshold field for breakdown at altitudes around 70 km where the z-component is pointing downward. From within this region, sprite streamer discharges are launched downward as positive streamers (not modeled), at times followed by negative streamers propagating upwards [*Cummer et al.*, 2006]. As mentioned earlier, streamers may propagate downward into regions with fields below the threshold because they carry their own space charge fields. Therefore, sprites are usually observed to extend below the altitudes of the high-field region shown in Figure 5. Since almost all sprites are generated by +CGs [*Boccippio et al.*, 1995; *Williams et al.*, 2007], it follows that this is the most common field configuration that initiates sprites.

[40] The electron density is shown in Figure 5 (right). It is the most important of the parameters that enter the electric conductivity and thereby affect the electric field. It is enhanced in the region that has been exposed to fields above the threshold, whereas in other regions it has decreased due to attachment, driven by fields just below the threshold. The region of enhanced ionization extends ~15 km in the vertical and ~40 km in the horizontal dimension. The region expands downward in time in the wake of the high fields until these are below the threshold. The volume of the atmosphere that may experience high electric fields depends on the +CG charge moment change and the time constant of the discharge (Q_c,τ_c) [*Pasko et al.*, 1998a, 1998b; *Li et al.*, 2008]. For the case we model here the high background electron density of $\sim 10^8$ m^{-3} at 90 km is extended down to approximately 70 km in the region above the +CG discharge. This is similar to the stronger cases of lightning given by *Pasko et al.* [1997, Figure 12].

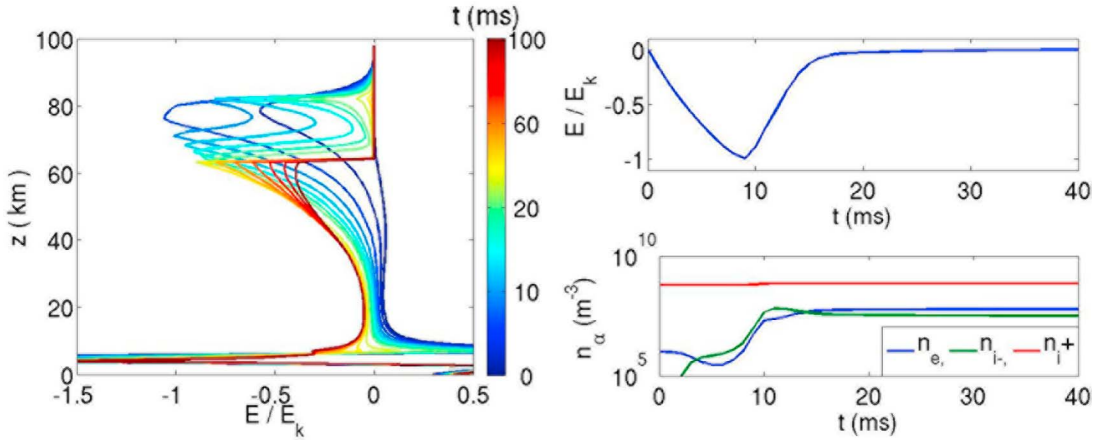

Figure 6. The time evolution of the normalized electric field and the densities for the cloud-to-ground discharge of Figure 5. (left) $E(t)/E_k$ on the axis of symmetry as a function of altitude. The curves are color coded marking the elapsed time in ms. The field peaks first at 78 km altitude. Then the peak splits in two because the enhanced ionization shorts out the field in this region. (right) The fields and the densities on the axis at 70 km altitude as functions of time.

[41] The time evolution of the fields and the densities are shown in Figure 6. Figure 6 (left) shows the normalized field on the axis as a function of altitude. The curves are color coded according to the time elapsed since the initiation of the cloud-to-ground discharge. The field in the mesosphere first increases, reaching a maximum around t = 6 ms with field amplitudes at ~80 km altitude close to, but above, E_k. The increase in the ionization (and electric conductivity) of the region causes a decrease of τ_σ and therefore an accelerated decrease of the electric field. Therefore, the field develops a structure with twin peaks, one above ~80 km altitude, and one moving downward with time. At later times, the field is completely shorted out in the region of enhanced ionization, with a sharp gradient at the lower edge at ~65 km altitude. When the gradients in the electric field and the densities become too large the model must be halted, as mentioned earlier (section 3.4).

[42] Figure 6 shows the electric field (Figure 6, top right) and the densities (Figure 6, bottom right) as functions of time for a fixed altitude of 70 km and on the axis of symmetry. The field first decreases, reaching a minimum close to the threshold field at ~9 ms, then increases again reaching zero at ~18 ms, which is also the value of τ_c and therefore close to the end of the cloud-to-ground discharge. The positive ion density, which has a finite value in our background model, is relatively unaffected by the electric field pulse. The negative ion density is governed by the attachment and detachment processes described in the previous section and their time constants. For small fields, the detachment time constant is smaller than the attachment time constant, and for large fields the opposite. Since the background negative ion density is initially zero, there is little detachment as the electric field pulse first increases in magnitude (negative). The negative ion density therefore increases because of attachment.

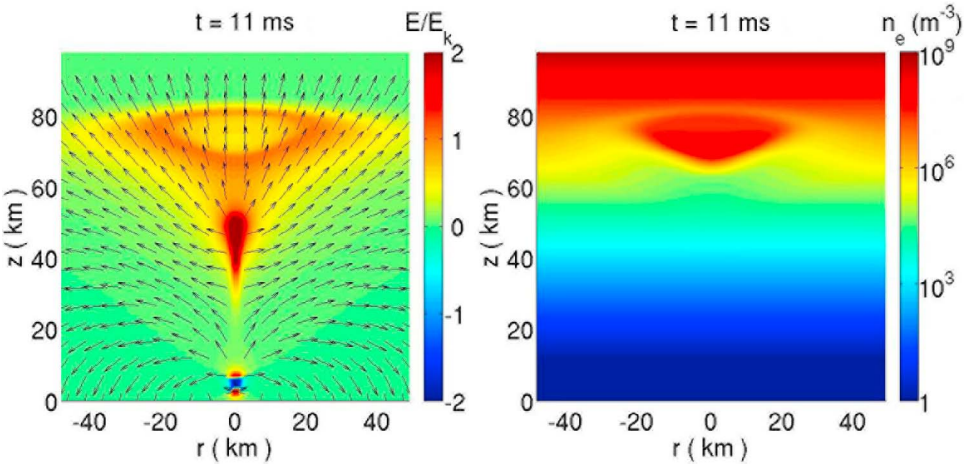

Figure 7. A giant at t = 11 ms when the leader has reached its fullest extent; $q_g^o = 8 \times 10^{-4}$ cm^{-1}, v_g = 4.7 × 106 ms^{-1}, and z_{gm} = 50 km. (left) The normalized electric field, E/E_k. (right) The electron density. The plots are in the same format as Figure 5.

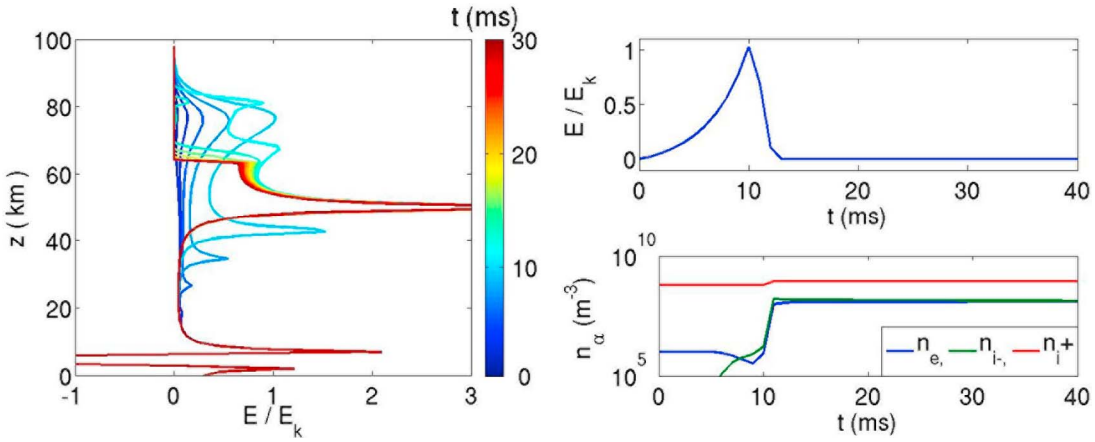

Figure 8. The time evolution of the normalized electric field and the densities for the giant of Figure 7. (left) $E(t)/E_k$ on the axis of symmetry as a function of altitude. The curves are color coded marking the elapsed time in ms. (right) The fields and the densities on the axis at 70 km altitude as functions of time.

Around $t \sim 5$ ms, the growth levels off because attachment and detachment begin to be comparable. As the field amplitude continues to increase (negative), we enter the high-field region where attachment and ionization dominates and the negative ion density rises faster again until it reaches a peak at ~11 ms, shortly after the peak of the electric field. When the pulse decreases in amplitude again, the negative ion density decreases for a short period because of detachment, reaching a steady value at ~18 ms. The electron density first decreases from its background value because of attachment. The decrease matches the increase of the negative ion density. The minimum value is reached at ~5 ms, where attachment and detachment are comparable. Then it increases rapidly because of increased ionization rates, reaching a steady value at ~18 ms where the field disappears. The elevated density is ~100 times the initial background density. Further discussion on the attachment and detachment processes are given in section 5.

4.2. Giant Only

[43] We next turn to the giant. Following [*Borovsky* [1998], we estimate the line charge density, q_g^o, from the assumption that the current $I_q = q_g^o v_g$. From Table 1 we find

$$q_g^o = 6.1 \times 10^{-4}\ \mathrm{Cm}^{-1} \text{ for P1 and } q_g{}^o = 8.5 \times 10^{-4}\ \mathrm{Cm}^{-1} \text{ for P2.}$$

[44] Since giants originate as lightning it is likely that the line charge density is within the range of lightning leaders, if indeed a giant is a leader. Several estimates of lightning charge densities per unit length along the lightning channel have been reported. In the summary of *Borovsky* [1998], stepped leaders are in the range 2×10^{-5} Cm^{-1} – 5×10^{-3} Cm^{-1}, depending on the method used to derive the estimates, and dart leaders 1×10^{-5} Cm^{-1} – 8×10^{-4} Cm^{-1}. In the work of *Rakov and Uman* [2003, pp. 125–126], the line charge density is estimated to 1×10^{-3} Cm^{-1} – 3.2×10^{-2} Cm^{-1}. The line charge density estimated from Table 1 is then within range of lightning leader densities. In the following we then adopt $q_g^o = 8 \times 10^{-4}$ Cm^{-1}, $v_g = 4.1 \times 10^6$ ms^{-1}, and $z_{gm} = 50$ km. The time it takes the stem to reach its maximum extent is then $t_r = z_{gm}/v_g = 12$ ms.

[45] The magnitude of the normalized electric field from the giant is shown in Figure 7 (left), at $t = 11$ ms, just around the time when the leader has reached its maximum vertical extent. In the mesosphere, the field has opposite polarity to the field of the +CG and the two fields may partly cancel here, if present simultaneously. The electric field is high around the tip of the giant stem, which compares well with the long-lasting, high-luminosity region of the giant seen in Figure 1, where high electric fields must be present. However, the tip field is not well represented in the model, as mentioned earlier.

[46] The corresponding electron density is shown in Figure 7 (right). The region of high electric fields and density enhancement in the mesosphere is smaller than for the case of the +CG because the source of the fields, the giant stem, rises closer to the mesosphere.

[47] The temporal evolution of the field and the densities are shown in Figure 8. The field on the axis (Figure 8, left) reaches values above the threshold field in the mesosphere during the upward propagation of the leader. The lower peak marks the altitude of the tip of the giant stem. The magnitude close to the stem is not well represented in the model, as mentioned earlier, and is sampled at 1-km distance from the axis. For the giant to propagate upwards from the cloud, the field at the tip must, of course, be above the threshold field. As for the +CG-field, the upper peak is reduced in regions where ionization is enhanced because of a decrease of the dielectric time constant. Therefore, the streamers of the mesosphere, the giant "canopy," are short-lived, as also observed.

[48] An interesting point to note here is that when the giant develops upwards, the normalized field first decreases with altitude from the tip, then increases again reaching a second maximum in the mesosphere. As mentioned earlier, streamers can, once formed, propagate at fields below the background field. For positive streamer propagation, the background field must be above $\sim E_k/7.3$ [*Moss et al.*, 2006]. Therefore, if the minimum of the normalized electric field between the tip and the mesosphere is above this value, then streamers launched from the tip can propagate the complete distance to the lower ionosphere. In other words, when the giant reaches a certain altitude propagating as a leader, it may jump as fast propagating streamers all the way to the

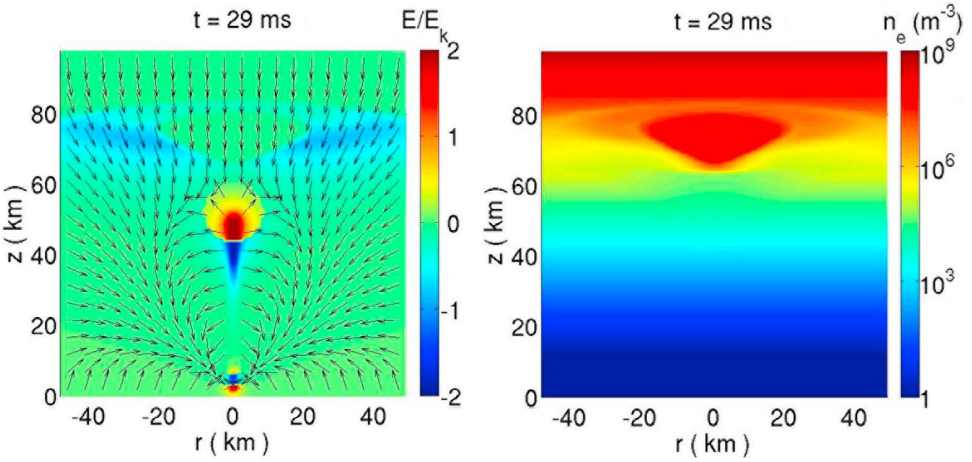

Figure 9. A giant followed by a positive cloud-to-ground discharge. The parameters are the same as in Figures 5 and 7. When the giant has reached its fullest extent at t = 11 ms, the cloud-to-ground discharge is initiated with τ_c = 18 ms. The plots show the (left) normalized electric field, E/E_k, and (right) electron density at t = 29ms.

ionosphere. This change in mode of propagation is consistent with observations in the past [*Pasko et al.*, 2002]. The altitude where this will happen depends, of course, on the charge carried by the jet. If it is low, streamers may never reach the ionosphere and the jet remains a blue jet or a blue starter. If it is high enough, it will develop into a giant. The streamer nature of the upper part of the giant is then the same as for sprites and thus sprites are in the same family as the upper reaches of a giant – at least for the positive polarity studied here. For negative polarity, a negative streamer requires the background field above $\sim E_k/2.6$ [*Moss et al.*, 2006], which suggests that a negative polarity giant may require a higher line charge density to form or must propagate to higher altitudes before it jumps to the ionosphere.

[49] The temporal evolution of the field on the axis at 70 km altitude is shown in Figure 8 (top right). The field pulse is of shorter duration than for the +CG, passing faster through the detachment – attachment regions of Figure 4. As for the +CG, detachment plays little role initially because there is no background O^- in the model. This ion density must first be created via attachment. The electron density at this location is also in this case enhanced by ~2 orders of magnitude.

[50] The currents (not shown) are flowing upwards, reaching $\sim 10^{-5}$ Am^{-2}. The current through 10 × 10 km^2, representing the cross section of the tip, is then ~1 kA which is about 1/3 the value of the current carried by the giant. In this region, streamers are formed (not modeled) that establish further ionization and currents above the tip (not modeled).

[51] We conclude, then, that observations so far seem to be consistent with the "stem" of the giant being of leader nature, establishing the necessary field amplitude to allow fast propagating streamers, the "canopy," to close the gap from the tip at 50 km and to the ionosphere.

4.3. Giant With a Sprite

[52] We now present the combined event of a giant and a sprite. We simplify the event to a single giant followed by a sprite. Both have the same parameter values as above, i.e., the values corresponding to P1 and P3. Since the parameters of the two pulses associated with the giant (P1 and P2) have almost the same values, it is not important which one is used to represent the giant event. The giant is launched into an unperturbed atmosphere and the +CG is started when the giant almost has reached its maximum extent at $t \sim 11$ ms. In this simplification we disregard that the giant is really stimulated twice (P1 and P2). It is clear from both the optical image of P2, which shows an absence of streamers in the mesosphere (the canopy), and from the VLF transmitter signal perturbation induced by the event [*van der Velde et al.*, 2010, Figure 8] that the perturbation to the mesosphere does not recover between P1 and P2. With the above simplification we may then underestimate the total perturbation to the mesosphere conductivity at the time of the +CG driving the sprite. The electric field of P1, however, will have relaxed to a low value above 60 km altitude at the time of P2/P3. The driving field is therefore best represented by the parameters of a single pulse.

[53] The combined field and electron densities are shown in Figure 9 at t = 29 ms ($\sim t_r + \tau_c$). The field is now reduced below the threshold in the region directly above the cloud where both fields independently have their maximum. High fields from the +CG are only obtained at some radial distance and at the lower edge of the region pre-ionized by the giant. It is from this region that sprite streamers are launched.

[54] Figure 10 shows the temporal evolution of the electric field and the densities. The on-axis field of the +CG (Figure 10, left) now passes through a negative maximum, narrow in altitude and centered on 83 km. The region of high field is reduced in vertical extent and the magnitude is below 0.8 E_k . The effect is caused by a combination of opposite polarity of the sprite and giant fields and the enhanced ionization caused by the giant, which screens out the field. For the combined event, the current changes polarity in the mesosphere (not shown), where the field of the +CG dominates. This is consistent with the polarity change of pulse P3.

[55] The temporal evolution at a fixed location at 70 km altitude on the axis is shown in Figure 10 (right). It resembles very much the situation of the giant (Figure 8) with little signature of the +CG. It means that the pre-ionization by the

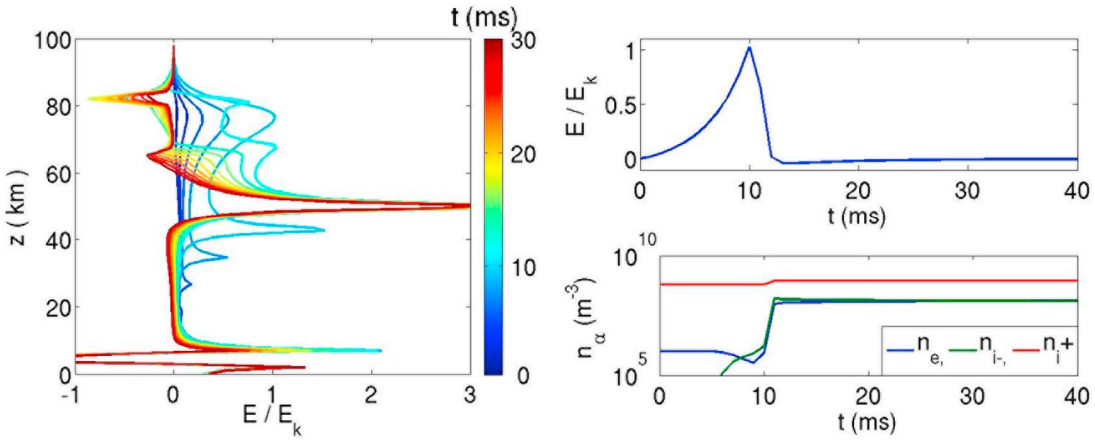

Figure 10. The time evolution of the normalized electric field and the densities for the giant followed by the cloud-to-ground discharge of Figure 9. (left) $E(t)/E_k$ on the axis of symmetry as a function of altitude. The curves are color coded marking the elapsed time in ms. (right) The fields and the densities on the axis at 70 km altitude as functions of time.

giant almost completely screens out the field of the +CG at this location. The only noticeable effect is a small excursion of the electric field to negative values at the end of the giant-pulse.

[56] We finally show for comparison the spatio-temporal evolution of the normalized field for the case of a +CG in an undisturbed atmosphere-ionosphere and for the case of a preexisting giant. The results are shown in Figure 11. Figure 11 (left) corresponds to the sprite case of Figure 5 and Figure 11 (right) to the combined case of Figure 9. The giant is first launched as before, then at $t = 11$ ms, close to the time of maximum excursion of the giant, the +CG is initiated. The times marked in Figure 11 are since the start of the +CG (Figure 11, left) and the giant (Figure 11, right).

[57] In the undisturbed case, the electric field is maximum on the axis of symmetry and is propagating downward. Sprite streamers are launched downward from this region (not modeled), taking a variety of forms, presumably depending on the fine structure of the region or of the electric field of the full electromagnetic pulse of a realistic lightning discharge. Figure 11 (right) shows the result with the giant. The electric field is in this case excluded in the region of high ionization and is moving outwards and downward around this region. Movies of the two cases are given as auxiliary material (see Animations S1 and S2).[1]

5. Discussion

5.1. Suppression of Sprites Near the Giant

[58] At an early stage of our modeling efforts the hypothesis was made that the exclusion of sprites at their usual location above a +CG was caused by the opposite polarity of the fields of the +CG and the giant in this region, leaving a generation region circling the giant at some distance. Running the code without perturbations to the atmosphere, we realized that a careful match of the source parameters is needed for this configuration to occur. With the complete model of the response of the atmosphere we found that the impulsive ionization of the central region by the field of the giant was far more effective in reducing the electric field of this region. The increase of the conductivity is fairly robust and the precise values of the parameters of the giant and +CG are not critical. As a consequence, the effect is not dependent on the polarity of the giant and should also occur for negative polarity giants.

[59] The relative magnitude of the fields of the +CG and the giant, and their time constants, determine parameters such as the radius of the sprite region and its altitude. The radial distance from the giant where emissions are suppressed is in our case ~20 km (Figure 9) which compares well with the observations (Figure 1c). The altitude is more difficult to assess since we do not follow the actual formation of streamers.

[60] We have assumed that the field driving the sprites is from a +CG discharge of a point charge in the cloud and that the location of this charge is on the axis of symmetry of the giant. Under this assumption the geometry of the volume in the mesosphere affected by the giant and the sprite fields is very similar and with a common axis of symmetry. If they are not aligned, or if the +CG is a result of horizontally extended spider lightning, the symmetry will be broken. In the case of the observations discussed here, the causative +CG is displaced ~20 km further away from the observation point along the line of sight [*van der Velde et al.*, 2010], suggesting the sprites probably are close to the giant but not necessarily circling it. The important aspects that we have accounted for with the model are therefore not the exact values of the discharge parameters or the geometry of the emissions but rather the absence of sprite emissions in a volume affected by the giant, which would otherwise be expected from this very intense +CG (196.8 kA peak current) with a large charge moment change.

[61] An alternative sprite generator mechanism could be the electromagnetic pulse (EMP) from the causative +CG, proposed by *Asano et al.* [2009] as the driver of ring structured clusters of column sprites [*Vadislavsky et al.*, 2009]. However, we find this mechanism unlikely to play a role in the event reported here. First, the +CG is so powerful, that large classic carrot sprites are to be expected and second, the

[1] Auxiliary materials are available in the HTML. doi:10.1029/2011JA016928.

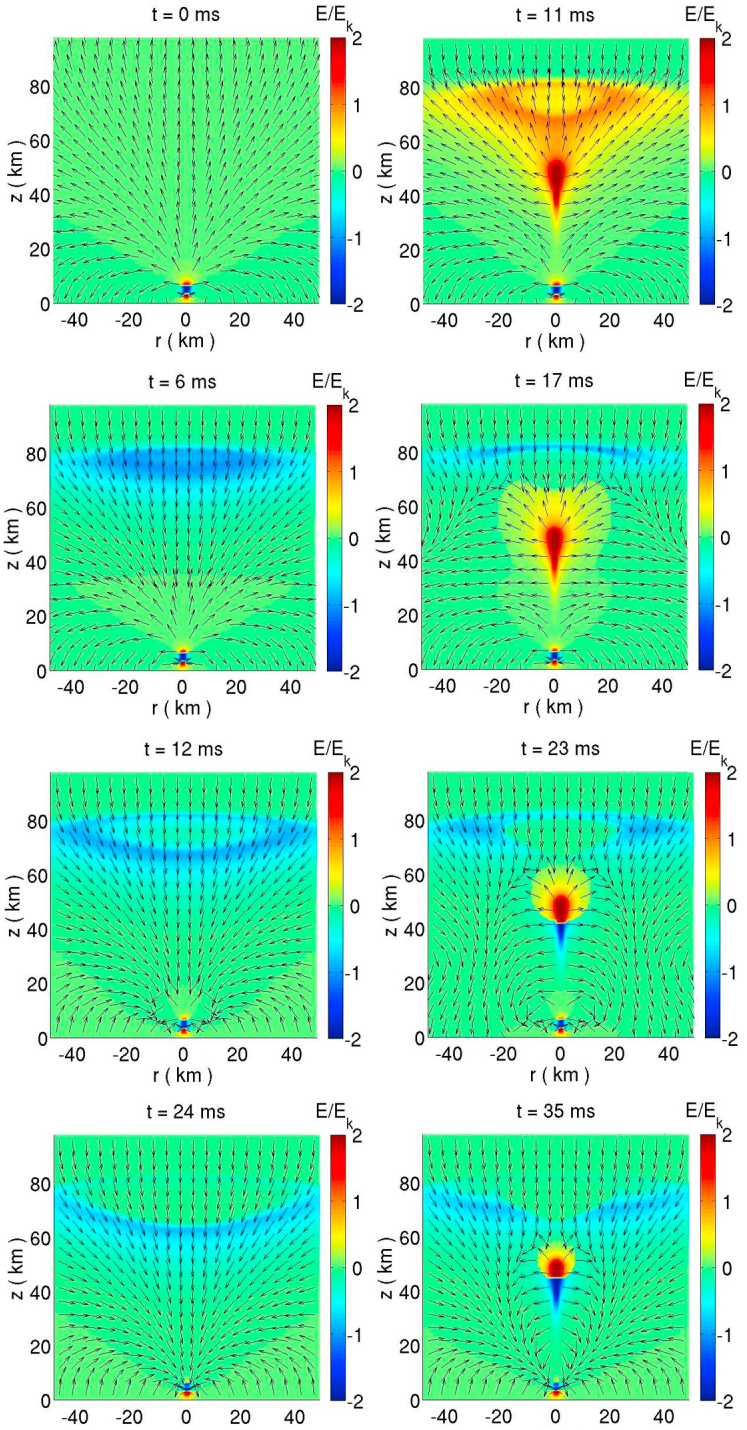

Figure 11. The spatiotemporal evolution of the normalized electric field from a positive cloud-to-ground discharge (left) without a giant and (right) with a pre-existing giant starting 11 ms earlier. Parameters are as in Figure 9. Times are relative to the start of the positive cloud-to-ground discharge (shown on the left) and the giant (shown on the right).

sprite elements of Figure 1 are different from column sprites, resembling instead dwarfed carrot sprite elements. We take this as an indication that their geometric organization indeed is caused by the perturbation to the mesosphere of the giant rather than the EMP of the causative +CG.

5.2. The Leader-Streamer Nature of a Giant

[62] Our first-principles model shows that the observed giant is consistent with a scenario where the "stem" is a leader with a line charge density of 0.8 mCm^{-1}, comparable to cloud-to-ground lightning densities, and the "canopy" is a short-lived multitude of streamers. We propose that in one

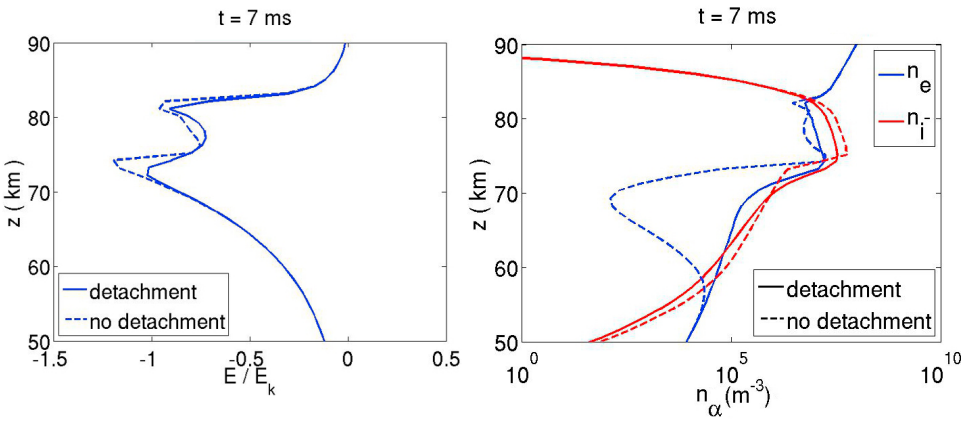

Figure 12. The role of detachment. A cloud-to ground discharge is initiated with the same parameters as in Figure 5. The (left) normalized electric field, E/E_k, and (right) electron and negative ion densities, ne,ni-, are shown along the axis of symmetry at $t = 7$ ms. The negative ion considered is O- Figure 12 (right), red curves. Full lines are for the detachment process from O- included, and dashed lines are without attachment.

limit, the potential carried by an upward propagating jet is insufficient to spark streamers traversing the mesosphere to the lower ionosphere, perhaps because the jet is of streamer nature or because the charge reservoir is insufficient. The jet then remains a blue jet or a blue starter. In another limit, a jet may carry sufficient potential such that streamers at some altitude are able to jump to the ionosphere, thus developing into a giant. The increased ionization of the streamers screens out the field of the region such that it cannot be maintained at high altitudes and only the "stem" remains. The long-lasting luminous region at 50–60 km altitude is the tip of the stem. Here a high electric field is maintained, providing currents between the stem and the upper atmosphere. This picture is in line with the mechanism suggested by *Raizer et al.* [2007] and *Milikh and Shneider* [2008].

[63] Our physical interpretation of the processes is different from the one presented by *Kuo et al.*[2009], where electron attachment is considered to dominate and therefore the conductivity is decreased above the jet. The leader mode of the stem then chases upwards toward an ionosphere boundary that also moves upwards because of increased electron attachment ahead of the jet. When the ionosphere eventually is reached they propose that a return stroke is triggered. The question of a return stroke is interesting but cannot be address by our model.

[64] The exact altitude of transition between leader and streamer will depend on the charge of the giant and its propagation speed (its impulsive nature), and of the dielectric time constant of the mesosphere. As a leader is propagating more slowly than a streamer, it is more susceptible to the decreasing dielectric time-constant with altitude which makes it progressively more difficult to maintain a high electric field. This process is seen to occur in Figure 8 (left), at ~70 km altitude and at the time of light blue curves (10–20 ms). At 70 km altitude the dielectric time constant of the background mesosphere is 10–100 ms for $E/E_k > 10^{-2}$ (Figure 4), which then represents an upper limit to the lifetime of the field of the stem at this altitude (not accounting for the added decrease in the time constant from streamer ionization).

[65] We note here that the vertical electric source field on the jet axis above the top of the jet stem ($z > z_{gm}$, $r \sim 0$) is $E_z \sim (z_{gm} - z_c)/((z-z_{gm})(z-z_c))$. The electric field of a line charge on, or close to, the axis is then decreasing less rapidly with altitude than the field of a spherical space charge (z^{-2}) or dipole (z^{-3}) often assumed for thunderclouds. The leader configuration of a jet/giant is therefore comparatively more effective in generating fields that allow streamers to propagate the full distance to the bottom ionosphere.

[66] To further explore the different modes of propagation, i.e., streamer versus leader, the velocity of propagation may be used as a discriminator. Studies of giants may therefore benefit from high temporal-resolution measurements. So far, array photometer observations have been applied to giants [*Kuo et al.*, 2009; *Chou et al.*, 2010] and high-speed imaging to sprites [*Stenbaek-Nielsen et al.*, 2007]. Bringing high-speed imaging to giants will allow resolving simultaneously their spatial and temporal dynamics, needed to firmly establish their streamer/leader nature and dependency on polarity.

5.3. The Detachment Process

[67] The dominant process that affects the atmospheric conductivity is ionization of atmospheric neutral constituents and attachment and detachment of electrons to/from molecular oxygen. On the time scales considered here, the currents conducted by positive and negative ions are small compared to the electron current, therefore the number of free electrons is of high importance to the physics of the region. An interesting point is that there seems to be a controversy concerning the detachment process. In the works of *Marshall et al.* [2008, 2010], *Kuo et al.* [2009], and *Lay et al.* [2010], electric field driven detachment is not considered and since the background detachment process has timescales of the order of 100 s or more at mesospheric altitudes [*Lehtinen and Inan*, 2007], this process is insignificant in the short-scale phenomena of discharges. However, the electric field-driven detachment rate for O^- has been measured by *Rayment and Moruzzi* [1978] and this process has been proposed by others to be a significant in the mesosphere [*Gordillo-Vázquez and Luque*, 2010; *Hiraki*, 2009].

[68] We illustrate the effect of detachment by repeating the simulation of a +CG without the detachment process. In Figure 12 (left), we show the electric field on the axis with and without detachment and in Figure 12 (right), we show the densities of electrons and O^- on the axis. Figure 12 (left) and Figure 12 (right) are for t = 7 ms. The electric field is seen to reach higher (negative) values when detachment is not present. In particular the lower peak is affected, where the no-detachment case overestimate the field by 25%. At this peak, the free electron density is larger with detachment, which tends to reduce the field magnitude. It is further seen, that without detachment the electron densities are severely reduced below 70 km because the field is below the breakdown field and electrons are removed by attachment.

[69] Without detachment the ionosphere will be depleted of electrons in regions of high electric fields, but below the threshold field. The same effect is seen in the work of *Marshall et al.* [2010], where the effect on the ionosphere of repeated lightning pulses (each below the threshold) is studied. Steep gradients in the electron density (and conductivity) develop at the lower edge of the ionosphere. Therefore, without detachment, we are not able to run the +CG model further than the 7 ms shown in Figure 12 because the gradients get too high for the code to handle. The highly dynamic field of a +CG (or a giant) is quite complex and Figure 12 only shows a snapshot. We expect the effect of no-detachment to be more pronounced, had we been able to simulate this condition further.

[70] The effect of detachment points to the need to rethink the meaning of the threshold electric field, E_k. It is often assumed that E_k is the field at which the ionization rate equals the attachment rate; rather it is the field where the ionization and detachment rates equal the attachment rate and therefore occurs at lower field values.

5.4. The Charge Density and Leader Potential

[71] We next discuss the charge density of the giant and show that the equivalent line charge of the stem it is consistent with our assumptions in the model, and that the potential of the tip and the total charge of the stem has reasonable values. The charge along the giant stem is, of course, not located along a line at the center, but distributed within the volume of the jet. Assuming the average radius to be $r_j \sim$ 5 km, the model line charge density of $q_g^o = 8 \times 10^{-4}\mathrm{Cm}^{-1}$ translates into an average volume charge density $\rho_g(z) \sim 1 \times 10^{-11}$ Cm^{-3}. An estimate of the charge density based on the observations can be derived from the properties of the glowing tip. At the terminal altitude at $z_{gm} \sim 50$ km, the vertical electric field must be of the order of the breakdown field for the atmosphere to continue to glow, or $\sim$2.25 kVm^{-1} at this altitude. The luminous region extends for about 10 km in the vertical direction. Noting that streamers, once formed, can propagate into regions with background fields below the threshold field where they constitute a luminous source, we assume that the field magnitude at the tip drops to a small value just above the tip over a vertical distance Δz that is smaller than 10 km. Assuming for instance $\Delta z \sim 2.25$ km, we find that the space charge density at the tip is $\rho_g(z) \sim \varepsilon_o E_k(z)/\Delta z \sim 1 \times 10^{-11}$ Cm^{-3}, which is consistent with the estimate of the line charge assumed in the model.

[72] With these assumptions we can also estimate the potential of the tip relative to the mesosphere. It is $\Delta\phi \sim E_k(z)\Delta z \sim 5$ MV, which is modest compared to the potential of the charge centers in clouds where the potential can reach several tens of MV relative to the ground or the ionosphere [*Rycroft et al.*, 2007; *Rycroft and Odzimek*, 2010], thus only a fraction of the cloud potential is brought up to 50 km altitude and the leader is not an ideal leader. We find that the total space charge in the giant stem is 44 C, or one third of the total charge neutralized in the cloud, which appears to be a reasonable value.

5.5. Thermal Expansion of the Giant Stem

[73] We next discuss the radial expansion of the giant stem and show that it is consistent with the interpretation of Joule heating. The typical radius of a leader in the troposphere is $\sim$0.1m [*Rakov and Uman*, 2003, p. 379]. As the radius of a leader is expected to be reversely proportional to the neutral gas density, this radius would correspond to $r_o(z)$ = 140 m at 50 km altitude, which is significantly lower than the observed radius. Supposing now that any segment of the giant leader stem below 50 km has been exposed to an average current I_a and an electric field $E = E_k$ for Δt seconds (the field must have reached this value, otherwise the jet would never have formed), then the energy deposited in the atmosphere in that segment is $P_W(z) \sim E_k(z) I_a \Delta t = (n_n(z)/n_n^o) E_k^o I_a \Delta t$, where n_n^o and E_k^o are the neutral density and the threshold field at sea level, respectively. With the radius expanding such that the deposited energy density equals the ambient energy density, we find $r_g(z)^2/r_o^2(z) = P_W(z)/P(z)$, where $P(z) = n_n(z) k T_n(z)$ is the background neutral energy density (pressure), or $r_g^2(z)/r_o^2(z) = E_k^o I_a \Delta t / n_o k T_n(z)$. This expression is weakly dependent on altitude which only appears via the temperature. At z = 50 km, with $\Delta t \sim 50$ ms and $I_a \sim 1.6$ kA as estimated from the ELF observations, we find that $P_W \sim 2 \times 10^5$ Jm^{-3} will be deposited at 50 km altitude. With the background gas energy density P = 72 Jm^{-3} (Pa) at this altitude, we find $r_g \sim 52\ r_o$ or $r_g \sim 7$ km, which is in good agreement with observations.

6. Concluding Remarks

[74] We have shown that the observations of displaced sprite elements in conjunction with a giant are consistent with a giant formed by a longer lasting positive leader "stem" and a short-lived streamer canopy. Our model of the event shows that the increased ionization and detachment by the leader field and of the streamer canopy creates enhanced conductivity that excludes the generation of sprites in a region close to the giant. A key point for the physics of giants is the role of attachment and detachment processes of the mesosphere driven by high electric fields. This issue is also important for other processes such as the repeated illumination of the lower ionosphere by electromagnetic pulses from lightning.

[75] The number of reported giants where their polarity is firmly established is limited to a few, so conclusions on which polarity is the most common and which conditions that create one versus the other needs more experimental evidence and improved models that follow up on such work as reported by *Krehbiel et al.* [2008] and others. The model we have presented here predicts that, once the initial leader of a jet has formed, a positive jet has a higher likelihood to

develop into a giant than a negative one. However, an important parameter is also the potential brought up across the stratosphere, here there could be a bias toward negative polarity giants.

[76] We finally comment that the giant jet discussed here was launched from surprisingly low clouds. This suggests that significant charge layers must have been present above the clouds at the tropopause or in the stratosphere. Such charge layers can be present as thin cirrus clouds, their ice crystals stabilized by electric charge [e.g., *Nielsen et al.*, 2007] or charged aerosols.

[77] **Acknowledgments.** We are grateful for valuable inputs on the detachment process by Alejandro Luque and Francisco J. Gordillo-Vazquez. The work received support from the NSF Physical and Dynamic Meteorology and Aeronomy Programs. E. Arnone acknowledges support by ESA within the framework of the Changing Earth Science Network Initiative. The collaboration was supported by the European Science Foundation through the Research Networking Programme: Thunderstorm Effects on the Atmosphere-ionosphere System (TEA-IS).

[78] Robert Lysak thanks the reviewers for their assistance in evaluating this paper.

References

Asano, T., T. Suzuki, Y. Hiraki, E. Mareev, M. G. Cho, and M. Hayakawa (2009), Computer simulations on sprite initiation for realistic lightning models with higher-frequency surges, *J. Geophys. Res.*, *114*, A02310, doi:10.1029/2008JA013651.

Boccippio, D. J., E. R. Williams, S. J. Heckman, W. A. Lyons, I. Baker, and R. Boldi (1995), Sprites, ELF transients and positive ground strokes, *Science*, *269*, 1088, doi:10.1126/science.269.5227.1088.

Borovsky, J. E. (1998), Lightning energetics: Estimates of energy dissipation in channels, channel radii, and channel-heating risetimes, *J. Geophys. Res.*, *103*(D10), 11,537–11,553, doi:10.1029/97JD03230.

Carlsen, T. (1967), *Elektricitetslære*, 472 pp., Akademisk Forlag, Copenhagen.

Chauzy, S., and S. Soula (1999), Contribution of the ground corona ions to the convective charging mechanism, *Atmos. Res.*, *51*, 279–300, doi:10.1016/S0169-8095(99)00013-7.

Cho, M., and M. J. Rycroft (1998), Computer simulation of the electric field structure and optical emission from cloud-top to the ionosphere, *J. Atmos. Sol. Terr. Phys.*, *60*, 871–888, doi:10.1016/S1364-6826(98)00017-0.

Chou, J. K., et al. (2010), Gigantic jets with negative and positive polarity streamers, *J. Geophys. Res.*, *115*, A00E45, doi:10.1029/2009JA014831.

Cummer, S. A., N. Jaugey, J. Li, W. A. Lyons, T. E. Nelson, and E. A. Gerken (2006), Submillisecond imaging of sprite development and structure, *Geophys. Res. Lett.*, *33*, L04104, doi:10.1029/2005GL024969.

Cummer, S. A., J. Li, F. Han, G. Lu, N. Jaugey, W. A. Lyons, and T. E. Nelson (2009), Quantification of the troposphere-to-ionosphere charge transfer in a gigantic jet, *Nat. Geosci.*, *2*, 617, doi:10.1038/ngeo607.

Davies, D. K. (1983), Measurements of swarm parameters in dry air, *Theor. Notes*, *346*, Westinghouse Electr., New York.

Gordillo-Vázquez, F. J., and A. Luque (2010), Electrical conductivity in sprite streamer channels, *Geophys. Res. Lett.*, *37*, L16809, doi:10.1029/2010GL044349.

Hiraki, Y. (2009), Effects of ion-neutral chemical reactions on dynamics of lightning-induced electric field, *Plasma Sources Sci. Technol.*, *18*, 034020, doi:10.1088/0963-0252/18/3/034020.

Krehbiel, P. R., J. A. Riousset, V. P. Pasko, R. J. Thomas, W. Rison, M. A. Stanley, and H. E. Edens (2008), Upward electrical discharges from thunderstorms, *Nat. Geosci.*, *1*(4), 233–237, doi:10.1038/ngeo162.

Kulikovsky, A. A. (1994), The structure of streamers in N, I: Fast method of space-charge dominated plasma simulation, *J. Phys. D Appl. Phys.*, *27*, 2556–2563, doi:10.1088/0022-3727/27/12/017.

Kuo, C.-L., et al. (2009), Discharge processes, electric field, and electron energy in ISUAL-recorded gigantic jets, *J. Geophys. Res.*, *114*, A04314, doi:10.1029/2008JA013791.

Lay, E. H., C. J. Rodger, R. M. Holzworth, M. Cho, and J. M. Thomas (2010), Temporal-spatial modeling of electron density enhancement due to successive lightning strokes, *J. Geophys. Res.*, *115*, A00E59, doi:10.1029/2009JA014756.

Lehtinen, N. G., and U. S. Inan (2007), Possible persistent ionization caused by giant blue jets, *Geophys. Res. Lett.*, *34*, L08804, doi:10.1029/2006GL029051.

Li, J., S. A. Cummer, W. A. Lyons, and T. E. Nelson (2008), Coordinated analysis of delayed sprites with high-speed images and remote electromagnetic fields, *J. Geophys. Res.*, *113*, D20206, doi:10.1029/2008JD010008.

Luque, A., and U. Ebert (2010), Sprites in varying air density: Charge conservation, glowing negative trails and changing velocity, *Geophys. Res. Lett.*, *37*, L06806, doi:10.1029/2009GL041982.

Marshall, R. A., U. S. Inan, and T. W. Chevalier (2008), Early VLF perturbations caused by lightning EMP-driven dissociative attachment, *Geophys. Res. Lett.*, *35*, L21807, doi:10.1029/2008GL035358.

Marshall, R. A., U. S. Inan, and V. S. Glukhov (2010), Elves and associated electron density changes due to cloud-to-ground and in-cloud lightning discharges, *J. Geophys. Res.*, *115*, A00E17, doi:10.1029/2009JA014469.

Milikh, G. M., and M. N. Shneider (2008), Model of UV flashes due to gigantic blue jets, *J. Phys. D Appl. Phys.*, *41*, 234013, doi:10.1088/0022-3727/41/23/234013.

Mishin, E. V., and G. M. Milikh (2008), Blue jets: Upward lightning, *Space Sci. Rev.*, *137*, 473–488, doi:10.1007/s11214-008-9346-z.

Moss, G. D., V. Pasko, N. Liu, and G. Veronis (2006), Monte Carlo model for analysis of thermal runaway electrons in streamer tips in transient luminous events and streamer zones of lightning leaders, *J. Geophys. Res.*, *111*, A02307, doi:10.1029/2005JA011350.

Neubert, T. (2003), On sprites and their exotic kin, *Science*, *300*(5620), 747–749.

Nielsen, J. K., N. Larsen, F. Cairo, G. Di Donfrancesco, J. M. Rosen, G. Durry, G. Held, and J. P. Pommereau (2007), Solid particles in the tropical lowest stratosphere, *Atmos. Chem. Phys.*, *7*, 685–695, doi:10.5194/acp-7-685-2007.

Pasko, V. P. (2003), The electric jet, *Nature*, *423*, 927–929, doi:10.1038/423927a.

Pasko, V. P. (2008), Blue jets and gigantic jets: Transient luminous events between thunderstorm tops and the lower ionosphere, *Plasma Phys. Control. Fusion*, *50*(12), 124050, doi:10.1088/0741-3335/50/12/124050.

Pasko, V. P., and J. J. George (2002), Three-dimensional modeling of blue jets and blue starters, *J. Geophys. Res.*, *107*(A12), 1458, doi:10.1029/2002JA009473.

Pasko, V. P., U. S. Inan, T. F. Bell, and Y. N. Taranenko (1997), Sprites produced by quasi-electrostatic heating and ionization in the lower ionosphere, *J. Geophys. Res.*, *102*(A3), 4529–4561, doi:10.1029/96JA03528.

Pasko, V. P., U. S. Inan, and T. F. Bell (1998a), Spatial structure of sprites, *Geophys. Res. Lett.*, *25*(12), 2123–2126, doi:10.1029/98GL01242.

Pasko, V. P., U. S. Inan, and T. F. Bell (1998b), Ionospheric effects due to electrostatic thundercloud fields, *J. Atmos. Sol. Terr. Phys.*, *60*, 863–870, doi:10.1016/S1364-6826(98)00022-4.

Pasko, V. P., U. S. Inan, and T. F. Bell (1999), Mesospheric electric field transients due to tropospheric lightning discharges, *Geophys. Res. Lett.*, *26*(9), 1247–1250, doi:10.1029/1999GL900240.

Pasko, V. P., M. A. Stanley, J. D. Matthews, U. S. Inan, and T. G. Wood (2002), Electrical discharge from a thundercloud top to the lower ionosphere, *Nature*, *416*, 152–154, doi:10.1038/416152a.

Raizer, Y. P. (1997), *Gas Discharge Physics*, Springer, Berlin.

Raizer, Y. P., G. M. Milikh, and M. N. Shneider (2006), On the mechanism of blue jet formation and propagation, *Geophys. Res. Lett.*, *33*, L23801, doi:10.1029/2006GL027697.

Raizer, Y. P., G. M. Milikh, and M. N. Shneider (2007), Leader–streamers nature of blue jets, *J. Atmos. Sol. Terr. Phys.*, *69*, 925–938, doi:10.1016/j.jastp.2007.02.007.

Rakov, V. A., and M. A. Uman (2003), *Lightning: Physics and Effects*, Cambridge Univ. Press, Cambridge, U. K.

Rayment, S. W., and J. L. Moruzzi (1978), Electron detachment studies between O^- ions nitrogen, *Int. J. Mass Spectrom. Ion Phys.*, *26*, 321–326, doi:10.1016/0020-7381(78)80033-3.

Riousset, J. A., and V. P. Pasko (2010), Modeling of thundercloud screening charges: Implications for blue and gigantic jets, *J. Geophys. Res.*, *115*, A00E10, doi:10.1029/2009JA014286.

Rycroft, M. J., and A. Odzimek (2010), The effects of lightning and sprites on the ionospheric potential, and threshold effects on spite initiation, obtained using an analog model of the global atmospheric electric circuit, *J. Geophys. Res.*, *115*, A00E37, doi:10.1029/2009JA014758.

Rycroft, M., A. Odzimek, N. F. Arnold, M. Füllekrug, A. Kulak, and T. Neubert (2007), New model simulations of the global atmospheric electric circuit driven by thunderstorms and electrified shower clouds: The roles of lightning and sprites, *J. Atmos. Sol. Terr. Phys.*, *69*, 2485–2509, doi:10.1016/j.jastp.2007.09.004.

Sentman, D. D., E. M. Wescott, D. L. Osborne, D. L. Hampton, and M. J. Heavner (1995), Preliminary results from the Sprites94 aircraft campaign: 1. red sprites, *Geophys. Res. Lett.*, *22*(10), 1205–1208, doi:10.1029/95GL00583.

Soula, S., O. van der Velde, J. Montanya, P. Huet, C. Barthe, and J. Bór (2011), Gigantic jets produced by an isolated tropical thunderstorm

near Réunion Island, *J. Geophys. Res.*, *116*, D19103, doi:10.1029/2010JD015581.

Stenbaek-Nielsen, H. C., M. G. McHarg, T. Kanmae, and D. D. Sentman (2007), Observed emission rates in sprite streamer heads, *Geophys. Res. Lett.*, *34*, L11105, doi:10.1029/2007GL029881.

Su, H. T., R. R. Hsu, A. B. Chen, Y. C. Wang, W. S. Hsiao, W. C. Lai, L. C. Lee, M. Sato, and H. Fukunishi (2003), Gigantic jets between a thundercloud and the ionosphere, *Nature*, *423*, 974–976, doi:10.1038/nature01759.

Vadislavsky, E., Y. Yair, C. Erlick, C. Price, E. Greenberg, R. Yaniv, B. Ziv, N. Reicher, and A. Devir (2009), Indication for circular organization of column sprite elements associated with eastern Mediterranean winter thunderstorms, *J. Atmos. Sol. Terr. Phys.*, *71*, 1835–1839, doi:10.1016/j.jastp.2009.07.001.

van der Velde, O. A., W. A. Lyons, T. E. Nelson, S. A. Cummer, J. Li, and J. Bunnell (2007), Analysis of the first gigantic jet recorded over continental North America, *J. Geophys. Res.*, *112*, D20104, doi:10.1029/2007JD008575.

van der Velde, O. A., J. Bór, J. Li, S. A. Cummer, E. Arnone, F. Zanotti, M. Füllekrug, C. Haldoupis, S. NaitAmor, and T. Farges (2010), Multi-instrumental observations of a positive gigantic jet produced by a winter thunderstorm in Europe, *J. Geophys. Res.*, *115*, D24301, doi:10.1029/2010JD014442.

Wescott, E. M., D. D. Sentman, D. L. Osborne, D. L. Hampton, and M. J. Heavner (1995), Preliminary results from the Sprites94 aircraft campaign: 2. Blue jets, *Geophys. Res. Lett.*, *22*(10), 1209–1212, doi:10.1029/95GL00582.

Wescott, E. M., D. D. Sentman, M. J. Heavner, D. L. Hampton, and O. H. Vaughan Jr. (1998a), Blue jets: Their relationship to lightning and very large hailfall, and their physical mechanisms for their production, *J. Atmos. Sol. Terr. Phys.*, *60*, 713–724, doi:10.1016/S1364-6826(98)00018-2.

Wescott, E. M., D. D. Sentman, M. J. Heavner, D. L. Hampton, W. A. Lyons, and T. Nelson (1998b), Observations of 'columniform' sprites, *J. Atmos. Sol. Terr. Phys.*, *60*, 733–740, doi:10.1016/S1364-6826(98)00029-7.

Williams, E. R. (2008), Atmospheric science: Predictable lightning paths?, *Nat. Geosci.*, *1*, 216–217, doi:10.1038/ngeo168.

Williams, E. R., E. Downes, R. Boldi, W. Lyons, and S. Heckman (2007), Polarity asymmetry of sprite-producing lightning: A paradox?, *Radio Sci.*, *42*, RS2S17, doi:10.1029/2006RS003488.

E. Arnone, ISAC-CNR, Via Gobetti 101, I-40129 Bologna, Italy. (e.arnone@isac.cnr.it)

O. Chanrion and T. Neubert, Division for Solar System Physics, National Space Institute, Technical University of Denmark, Juliane Maries vej 30, Building Rockefeller, Rm. 2–101, Copenhagen D-2100 KBH Ø, Denmark. (chanrion@space.dtu.dk; neubert@space.dtu.dk)

S. Cummer and J. Li, Department of Electrical and Computer Engineering, Duke University, PO Box 90291, Durham, NC 27708, USA. (cummer@ee.duke.edu; jingbo.li@duke.edu)

M. Füllekrug, Centre for Space, Atmospheric and Oceanic Science, Department of Electronic and Electrical Engineering, University of Bath, Bath BA2 7AY, UK. (eesmf@bath.ac.uk)

S. Soula, OMP, Laboratoire d'Aérologie, Université Paul Sabatier de Toulouse, CNRS, 14 Ave. Edouard Belin, Toulouse F-31400, France. (us@aero.obs-mip.fr)

O. van der Velde, Electrical Engineering Department, Technical University of Catalonia, 1 Colon, E-08222 Terrassa, Spain. (oscar.van.der.velde@upc.edu)

F. Zanotti, Via G. Magoni 21, I-44124 Ferrara, Italy. (fzanotti1@alice.it)